Stability of a Rh/CeO_2-ZrO_2 Catalyst in the Oxidative Steam Reforming of Raw Bio-oil

Remiro, Aingeru; Arandia, Aitor; Oar-Arteta, Lide; Bilbao, Javier; Gayubo, Ana G.

DOI
10.1021/acs.energyfuels.7b04141

Publication date
2018

Document Version
Final published version

Published in
Energy and Fuels

energy&fuels

Article

Cite This: Energy Fuels 2018, 32, 3588−3598

pubs.acs.org/EF

Stability of a Rh/CeO_2−ZrO_2 Catalyst in the Oxidative Steam Reforming of Raw Bio-oil

Aingeru Remiro,*[,†] Aitor Arandia,[†] Lide Oar-Arteta,[‡] Javier Bilbao,[†] and Ana G. Gayubo[†]

[†]Chemical Engineering Department, University of the Basque Country, P.O. Box 644, 48080 Bilbao, Spain

[‡]Faculty of Applied Sciences, Chemical Engineering, Delft University of Technology, Building 58, Van der Maasweg 9, Delft, Netherlands

Supporting Information

ABSTRACT: The oxidative steam reforming (OSR) of raw bio-oil (obtained by fast pyrolysis of pine sawdust) has been studied on a Rh/CeO_2−ZrO_2 catalyst under a wide range of operating conditions (600−750 °C; steam-to-carbon molar ratio, 3−9; oxygen-to-carbon molar ratio, 0.34; space time, 0.15−0.6 $g_{catalyst}$ h/$g_{bio\text{-}oil}$) in order to delimit the suitable conditions for high and stable H_2 production. The runs were conducted in a two-step system provided with a thermal step (at 500 °C) for bio-oil vaporization and pyrolytic lignin retention, followed by an online catalytic reforming step in a fluidized bed reactor. The spent catalyst was characterized by temperature-programmed oxidation, temperature-programmed reduction, and transmission electron microscopy in order to ascertain the causes of deactivation and the effect of the reaction conditions on these causes. The evolution with time on stream of both bio-oil oxygenates conversion and yields of reaction products shows different periods and catalyst states, with two sharp changes associated with different catalyst deactivation causes: (i) change in the states of Rh species and aging of the support (with fast dynamics) and (ii) coke deposition (at low temperature) or Rh sintering (at high temperature, with slow dynamics).

1. INTRODUCTION

The need to reduce greenhouse gas emissions calls for the urgent development of sustainable energy-generating processes.[1] Within this scenario, H_2 has great potential as an energy carrier for progressively replacing fossil fuels, with the main sources for its production currently being natural gas, oil-derived hydrocarbons, and coal. The technological development of biomass-derived H_2 production is therefore receiving particular attention in the quest to reduce net emissions of CO_2.[2−4]

The steam reforming (SR) of bio-oil (the liquid product of biomass pyrolysis) has great potential for H_2 production. The stoichiometry of this reaction [considering the water gas shift (WGS) reaction] is as follows:

$$C_nH_mO_k + (2n - k)H_2O \rightarrow nCO_2 + (2n + m/2 - k)H_2 \quad (1)$$

H_2 production through this route is of great interest because the steps of biomass pyrolysis and bio-oil reforming involve advantages over other alternatives for the production of H_2 from biomass: (i) The energy required for biomass drying is saved because the feed may contain the moisture corresponding to ambient conditions. (ii) The bio-oil may be produced at a high yield at the place where the biomass is located (avoiding transportation) by fast pyrolysis of any biomass feed using low environmental impact technologies.[5−8] (iii) The energy required for pyrolysis and product condensation may be reduced by conducting the process under vacuum,[9] with no energy requirements when the process is carried out under autothermal regime (oxidative pyrolysis) and product composition being similar.[10] (iv) The steam reforming process does not require the dehydration of bio-oil and may be carried out at large scale to produce high-purity H_2 with the yield being almost that corresponding to stoichiometry.[11−14] (v) The external energy supply for bio-oil reforming is avoided by performing oxidative steam reforming (OSR) in which the heat absorbed is supplied by the partial combustion of the components in the reaction medium by cofeeding a given O_2 flow rate. With an appropriate O (oxygen)/S(steam)/C ratio in the OSR process, the autothermal reforming (ATR) regime is achieved, which is suitable for use in small reforming units when there are energy supply limitations.[15] The global stoichiometry of the OSR for bio-oil is as follows:

$$C_nH_mO_k + pO_2 + (2n - k - 2p)H_2O \rightarrow nCO_2 + (2n + m/2 - k - 2p)H_2 \quad (2)$$

One of the factors conditioning the industrial implementation of the catalytic processes for the valorization of the bio-oil is the rapid deactivation of the catalyst due to the repolymerization of phenolic compounds present in the bio-oil. This problem has been partially solved by the controlled polymerization of the pyrolytic lignin in a step prior to the reforming reactor. This technology has been successfully used in the production of hydrocarbons and in the SR of bio-oil.[16,17] Furthermore, the partial combustion of the intermediates leading to coke formation in the OSR regime hinders catalyst deactivation to some extent.[18−20] However, the major limitation of bio-oil OSR is that equilibrium H_2 yield is lower

Received: December 29, 2017
Revised: February 21, 2018
Published: February 21, 2018

DOI: 10.1021/acs.energyfuels.7b04141
Energy Fuels 2018, 32, 3588−3598

than that in the SR, i.e., around 20% lower according to the thermodynamic analysis conducted by Vagia et al.[21]

OSR reaction has been mainly studied for ethanol,[22−26] hydrocarbons,[27−30] and model oxygenates of bio-oil.[16,31,32] Few studies deal with the OSR of bio-oil or its aqueous fraction.[15,18,33,34] In all these studies, low-cost Ni catalysts have been used in the OSR, which are well-established catalysts for the SR.[35−37] Although noble metal-based catalysts are more expensive, they are more stable. The better behavior of Rh over Ni-based catalysts has been proven for the reforming of pure oxygenates, such as ethanol and glycerol.[38,39] Recently, the authors of this work studied the OSR of raw bio-oil and proved the superior behavior of a $Rh/CeO_2{-}ZrO_2$ catalyst over a Ni-based one.[40] The suitable conditions toward high H_2 yield were determined,[41] and the significant attenuating effect on coke deposition was proven for high oxygen/carbon (O/C) ratios in the feed due to the partial combustion of coke precursors.[40]

In these previous studies[40,41] it was proven that the catalyst undergoes deactivation due to several possible causes, such as coke deposition, oxidation, and/or catalyst sintering. The deactivation rate and the relative importance of these causes depend on the operating conditions (temperature, space time, and steam/oxygen/carbon ratio in the feed). The effect of the O/C ratio on the catalyst deactivation was studied in depth in our previous work for a given set of the remaining operating conditions.[40] Given the importance of catalyst stability for the viability of the OSR of bio-oil, the objective of this work is to analyze the effect the remaining operating conditions (temperature, space time, and S/C ratio in the feed) have on the stability of the $Rh/CeO_2{-}ZrO_2$ catalyst. Moreover, the causes of its deactivation and their relative importance have been determined in different reaction conditions in order to determine the optimum reaction conditions for minimizing deactivation.

2. EXPERIMENTAL SECTION

2.1. Catalyst. A commercial $Rh/CeO_2{-}ZrO_2$ catalyst was used, with 2 wt % Rh content, which was supplied by Fuel Cell Materials. The specific surface area, average pore diameter, and pore volume (determined by N_2 adsorption−desorption, in an Autosorb iQ2 equipment from Quantachrome) were 85.7 $m^2\ g^{-1}$, 17.7 nm, and 0.31 $cm^3\ g^{-1}$, respectively. A metal dispersion of 72.5% and a metallic surface area of 319 $m^2\ g_{metal}{}^{-1}$ were determined by CO chemisorption (Autosorb iQ2 from Quantachrome). The temperature-programmed reduction (TPR) profile was obtained in a Micromeritics AutoChem 2920. In the procedure, the sample (100−200 mg) was under a He flow (200 °C, 1 h), and it was subsequently reduced in 50 cm^3/min of 10 vol % H_2/Ar mixture, with a heating ramp of 7 °C/min from 30 to 900 °C. The TPR profile shows that Rh_2O_3 is fully reduced below 250 °C (section 3.2.2). The X-ray diffraction (XRD) results (Bruker D8 Advance diffractometer) confirm the presence of Ce and Zr oxides, but no diffraction peaks corresponding to Rh_2O_3 (prior to reduction) or Rh^0 (after reduction) are observed which is due to the low Rh content and its high dispersion on the support.[40] The Rh particle size distribution of the fresh catalyst was estimated from transmission electron microscopy (TEM) images obtained in a Philips SuperTwin CM200, and the values vary from 1 to 2.5 nm.[41]

The amount and nature of the coke deposited on spent catalysts has been determined by temperature-programmed oxidation (TPO) in a Thermo Scientific TGA Q5000TA thermobalance. In the procedure, after the temperature stabilizes at 50 °C, 50 cm^3/min of N_2/O_2 (25 vol % of O_2) was fed and heated to 800 °C with a heating ramp of 10 °C/min.

2.2. Bio-oil Production and Composition. The raw bio-oil was obtained by flash pyrolysis of pine sawdust at 480 °C in a semi-industrial demonstration plant (Ikerlan-IK4 technology center, Alava, Spain), with a biomass feeding capacity of 25 kg/h.[42] The water content of the bio-oil is 38 wt %; its density is 1.107 g mL^{-1}, and the empiric formula obtained by CHO analysis is $C_{4.21}H_{7.14}O_{2.65}$ (water-free basis). The raw bio-oil composition, determined by GC/MS analyzer (Shimadzu QP2010S device), has been reported elsewhere.[40]

2.3. Reaction Equipment, Operating Conditions, and Reaction Indices. Runs have been performed in an automated reaction equipment of stainless steel (MicroActivity Reference from PID Eng&Tech) provided with two units in series (thermal step and catalytic step), which has been described in detail in a previous work.[40] The thermal step consists of a U-shaped tube for repolymerization of the oxygenates derived from lignin pyrolysis. The thermal unit (U-tube) has a high section in order to extend the time of use until it gets blocked. This blockage does not take place under the conditions studied here but will unavoidably occur at longer reaction times. This problem can be solved by giving the feed access to another thermal unit. Thus, while in one of the units the pyrolytic lignin is being deposited, in the other unit it is being removed. In a previous work, different valorization routes were proposed for this pyrolytic lignin, based on its composition and properties.[43]

In this study, the thermal unit operates at 500 °C, which is the optimum temperature for maximizing the bio-oil fraction liable to valorization in the subsequent reforming reactor, because it attains the best compromise between pyrolitic lignin deposition (which increases noticeably below 500 °C) and oxygenates cracking to CO, CH_4, and $C_2{-}C_3$ hydrocarbons (which increases exponentially above 500 °C). Moreover, it leads to a better compromise between H_2 yield and catalyst stability in the subsequent reforming step, because the resulting oxygenate composition causes less deactivation of the reforming catalyst.[44] In this thermal step, around 11 wt % of the raw bio-oil oxygenates, or 18.6 wt % of C in the bio-oil feed (both values on a water-free basis), was deposited as pyrolytic lignin [which corresponds to a constant deposition rate of 2.59 mg/min, for the bio-oil feeding rate used of 0.08 mL/min (water included)].

The molecular formula corresponding to the bio-oil exiting the thermal step is $C_{3.8}H_{7.7}O_{2.9}$ (water-free basis, calculated from a mass balance based on the molecular formula of the raw bio-oil and the amount and composition of the pyrolytic lignin deposited). The composition of the volatile stream at the outlet of the thermal unit (or at the catalytic reactor inlet) remains constant with the time on stream. This composition depends on the operating conditions of the thermal treatment, especially on temperature, but with low dependence on the S/C ratio for the bio-oil used in this work. In the second unit (catalytic reforming reactor in fluidized bed regime), the catalyst is mixed with inert solid (SiC) (inert/catalyst mass ratio > 8/1) in order to ensure a correct fluidization regime. It should be noted that the O_2 feed was placed just at the reactor entrance in order to prevent the oxidation of the bio-oil in the first step (thermal treatment), thus maximizing the H_2 yield in the two-step reaction system.[45] Prior to each reforming reaction, the catalyst is reduced in situ in a $H_2{-}N_2$ stream (10 vol % H_2) at 700 °C for 2 h. The reactions have been carried out at atmospheric pressure, with the remaining operating conditions as follows: 600−750 °C; space time between 0.15 and 0.6 $g_{catalyst}\ h/g_{bio\text{-}oil}$; steam/carbon (S/C) molar ratio in the 3−9 range, which is obtained by cofeeding water (307 Gilson pump) with the raw bio-oil (injection pump Harvard Apparatus 22); oxygen/carbon ratio (O/C), 0.34. This O/C ratio is suitable for achieving a good balance between the two opposite effects due to the cofeeding of O_2:[40] on the one hand, it attenuates deactivation by preventing coke formation; on the other hand, it provokes a decrease in H_2 yield due to a higher extent of oxidation reactions of oxygenates over the reforming reactions.

The product stream is analyzed in-line with a MicroGC 490 from Agilent, equipped with four analytic channels: molecular sieve MS5 for quantifying H_2, N_2, O_2, CH_4 and CO; Plot Q for CO_2, H_2O, and $C_2{-}C_4$ hydrocarbons; CPSIL for $C_5{-}C_{11}$ hydrocarbons (not detected in this study); and Stabilwax for oxygenated compounds.

The following reaction indices have been used for quantifying the kinetic behavior:

DOI: 10.1021/acs.energyfuels.7b04141
Energy Fuels 2018, 32, 3588−3598

$$\text{Bio-oil conversion: } X_{\text{bio-oil}} = \frac{F_{\text{in}} - F_{\text{out}}}{F_{\text{in}}} \quad (3)$$

where F_{in} and F_{out} are the molar flow rates of bio-oil oxygenates at the reactor inlet and outlet, respectively, in C units contained. The C molar flow-rate of bio-oil oxygenates at the reactor inlet (F_{in}) has been calculated by a mass balance, taking into account the amount of bio-oil oxygenates retained (as pyrolytic lignin) in the thermal step. The C molar flow-rate of bio-oil oxygenates at the outlet of the reactor (F_{out}) has been calculated from the molar fraction of individual oxygenates (determined by microGC analysis) and the total mole number in the outlet stream, determined by C mass balance for the reforming reactor.

$$\text{H}_2 \text{ yield: } Y_{\text{H}_2} = \frac{F_{\text{H}_2}}{F^0_{\text{H}_2}} \quad (4)$$

where F_{H_2} is the H_2 molar flow rate in the product stream and $F^0_{\text{H}_2}$ is the stoichiometric molar flow rate, which has been evaluated for the SR reaction as $(2n + m/2 - k)/n \cdot F_{\text{in}}$, according to eq 1. Taking into account the molecular formula of the bio-oil oxygenates entering the reforming reactor ($C_{3.8}H_{7.7}O_{2.9}$), this value of $F^0_{\text{H}_2}$ is $2.25F_{\text{in}}$.

The yield of carbon-containing products (CO_2, CO, CH_4, and light hydrocarbons) is

$$Y_i = \frac{F_i}{F_{\text{in}}} \quad (5)$$

where F_i is the molar flow rate of each compound, in C units contained.

CH_4 and light hydrocarbons (mainly ethane) are formed by the thermal decomposition of bio-oil oxygenates:

$$C_nH_mO_k \rightarrow C_xH_yO_z + \text{gases}(H_2, CO, CO_2, CH_4) + \text{coke} \quad (6)$$

The relative significance of these secondary reactions in the OSR decreases under certain conditions, such as high space time, which favor the extent of the catalyzed reaction (reforming and WGS).[41]

3. RESULTS

3.1. Effect of Reaction Conditions on Catalyst Stability. *3.1.1. Space Time.* Figure 1 shows the effect of space time on the evolution with TOS of bio-oil conversion and H_2 yield (graph a), CO_2 and CO yields (graph b), and CH_4 and light hydrocarbons yields (graph c). These results correspond to experiments conducted at 700 °C, O/S/C = 0.34/6/1 molar ratio in the feed, and two space time values of 0.15 and 0.60 g_{catalyst} h/$g_{\text{bio-oil}}$. A low space time allows studying deactivation at relatively low TOS (10 h). As observed, at low space time (blue dots in Figure 1) catalyst deactivation is fast in two different periods leading to two sharp changes. As will be explained in section 4, this is due to different deactivation causes. During the first period the decrease in the conversion of bio-oil oxygenates and H_2 (Figure 1a) and CO_2 (Figure 1b) yields is not very pronounced, which is attributed to the slight catalyst deactivation for the reforming of oxygenates (eq 2) and the WGS reaction. Moreover, in this first deactivation period, CH_4 and hydrocarbon (HC) yields increase with TOS because of the catalyst deactivation for their reforming, with the reforming of CH_4 being more affected and its concentration increasing faster.

After the first deactivation period, the catalyst reaches a pseudostable state. During this period the conversion remains almost constant and the H_2, CO_2, and HCs yields vary slowly. After 150 min TOS, a fast deactivation starts (second sharp change), in which the conversion of oxygenates and the H_2 and CO_2 yields decrease and the yield of HCs increases. These

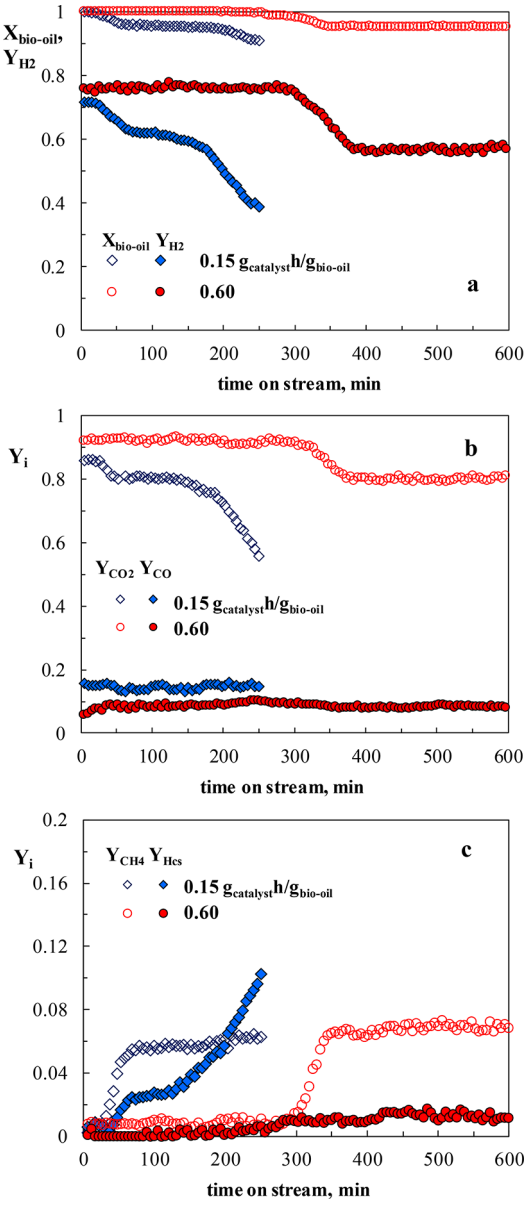

Figure 1. Effect of space time on the evolution with TOS on bio-oil oxygenates conversion and H_2 yield (a) and on the yields of carbon-containing products (b and c). Reaction conditions: 700 °C; O/C, 0.34; S/C, 6.

results are likely due to a decrease in the catalyst activity for the reforming of oxygenates and hydrocarbons and the WGS reaction. Nonetheless, CH_4 yield remains almost constant during this period. Its value of 0.06 is close to that obtained by bio-oil decomposition without a catalyst at the same temperature.[41] This evidences the almost total catalyst deactivation for the reforming of CH_4 during the first deactivation period (first sharp change in Figure 1).

For the highest space time, results are different from those aforementioned (red dots in Figure 1). In this case, a delay is observed for the first sharp change, and the second is not observed. The delay in the first sharp change, which is almost proportional to the increase in space time, is attributed to the high activity of the catalyst which is in excess; thus, the deactivation hardly affects the composition of the product stream over 300 min TOS. During the fast deactivation period, the reaction indices vary significantly with TOS, in a way similar

DOI: 10.1021/acs.energyfuels.7b04141
Energy Fuels 2018, 32, 3588−3598

to those for low space time in the first sharp change. Subsequently, the reaction indices remain constant over 24 h TOS (as previously reported by the authors).[40] All this evidences that a high space time delays the consequences of deactivation and, apparently, also its causes.

Another remarkable aspect of the results in Figure 1 is that CO yield (Figure 1b) remains almost constant with TOS for both space times. This is because CO is an intermediate in the kinetic scheme of the reaction.[41] According to this scheme, CO is the product of the catalyzed reforming and oxidation reactions and the reactant in the WGS reaction. Thus, as a consequence of the deactivation, its formation (reforming reaction) and conversion (WGS) are both attenuated. Accordingly, its yield remaining constant is due to the fact that the deactivation effect is similar on the reforming and the WGS reactions, which corresponds to a nonselective deactivation mechanism. Moreover, the deactivation of the WGS reaction for this catalyst is presumably slow because of the well-established contribution of CeO_2 in the support to the WGS reaction.[46]

3.1.2. Temperature. Figure 2 shows the evolution of bio-oil conversion and product yields with TOS at 600 and 750 °C, O/S/C = 0.34/6/1 molar ratios in the feed, and low space time (0.15 $g_{catalyst}$ h/$g_{bio\text{-}oil}$); thus, deactivation is fast, as proven in section 3.1.1.

At high temperature (750 °C) the two sharp changes observed at 700 °C for the same space time (blue dots in Figure 1) can be distinguished, corresponding to two deactivation periods due to different causes. The first period, in which deactivation is fast, takes place at 30−60 min TOS, and the second period starts at 200 min, with little impact on deactivation. It is noteworthy that the duration of the pseudostable period between both sharp changes is higher at 750 °C (red dots in Figure 2) than at 700 °C (blue dots in Figure 1).

Unlike the results at 700 and 750 °C, Figure 2 shows only one sharp change at 600 °C, after 50 min TOS; a fast and pronounced decrease in the H_2 (Figure 2a) and CO_2 (Figure 2b) yields takes place simultaneously with a fast increase in CH_4 and hydrocarbon yields (Figure 2c). After 100 min TOS the yields of products evolve very slowly. CH_4 and hydrocarbon yields are almost constant (specially the former) and similar to those obtained via the decomposition of oxygenates from bio-oil by thermal routes,[41] thereby evidencing almost full catalyst activity loss for the reforming of these compounds. Nevertheless, the catalyst keeps residual activity for oxidation reactions and the reforming of the oxygenates of bio-oil and the WGS reaction. As a consequence, CO yield is lower than the one corresponding to decomposition of oxygenates, and H_2 and CO_2 yields are higher. Presumably, the support plays a role in the residual activity of the catalyst, as previously commented.[46] Otherwise, the existence of a sole sharp change at 600 °C is likely due to the absence of one of the deactivation causes at this temperature or to the overlapping of both sharp changes, because these deactivation causes happen at the same time.

The results in Figure 2 and those corresponding to low space time at 700 °C (blue dots in Figure 1) highlight the low dependence of deactivation on temperature during the first sharp change. Moreover, the second change is less pronounced with increasing temperature (especially from 600 to 700 °C), thus indicating the limitation of the corresponding deactivation mechanisms.

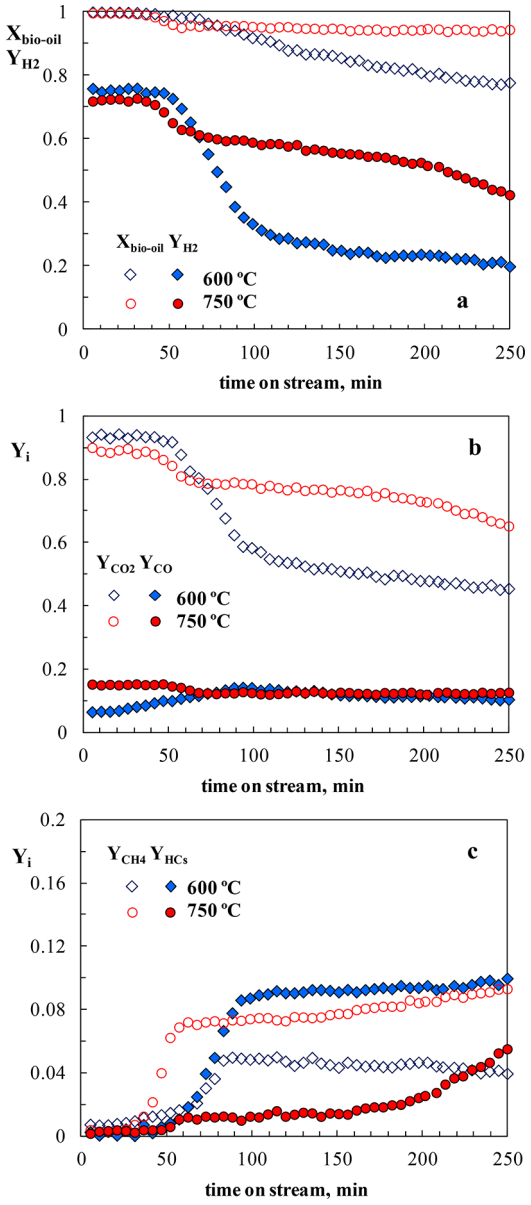

Figure 2. Effect of temperature on the evolution with TOS on bio-oil oxygenates conversion and H_2 yield (a) and on the yields of carbon-containing products (b and c). Reaction conditions: space time, 0.15 $g_{catalyst}$ h/$g_{bio\text{-}oil}$; O/C, 0.34; S/C, 6.

3.1.3. S/C Ratio. Figure 3 shows the effect of S/C ratio on the evolution with TOS of the reaction indices. The other reaction conditions are as follows: space time, 0.15 $g_{catalyst}$ h/$g_{bio\text{-}oil}$; 700 °C; O/C molar ratio, 0.34. For both S/C ratios, two sharp changes or deactivation periods are observed. When the S/C ratio is increased, the impact of deactivation on the yields of different products is higher and the pseudostable period after the first sharp change lasts longer. For S/C = 9, the second sharp change takes place after 220 min TOS, and for S/C = 3 after 100 min, with a continuous decrease in H_2 (Figure 3a) and CO_2 (Figure 3b) yields and a steady increase in the hydrocarbons yield (Figure 3c). These results evidence that the progress of deactivation during the second period (second sharp change) is notably attenuated by increasing the S/C ratio.

3.2. Analysis of Deactivation Causes. Complementary techniques have been used to characterize the catalyst, thus

DOI: 10.1021/acs.energyfuels.7b04141
Energy Fuels 2018, 32, 3588−3598

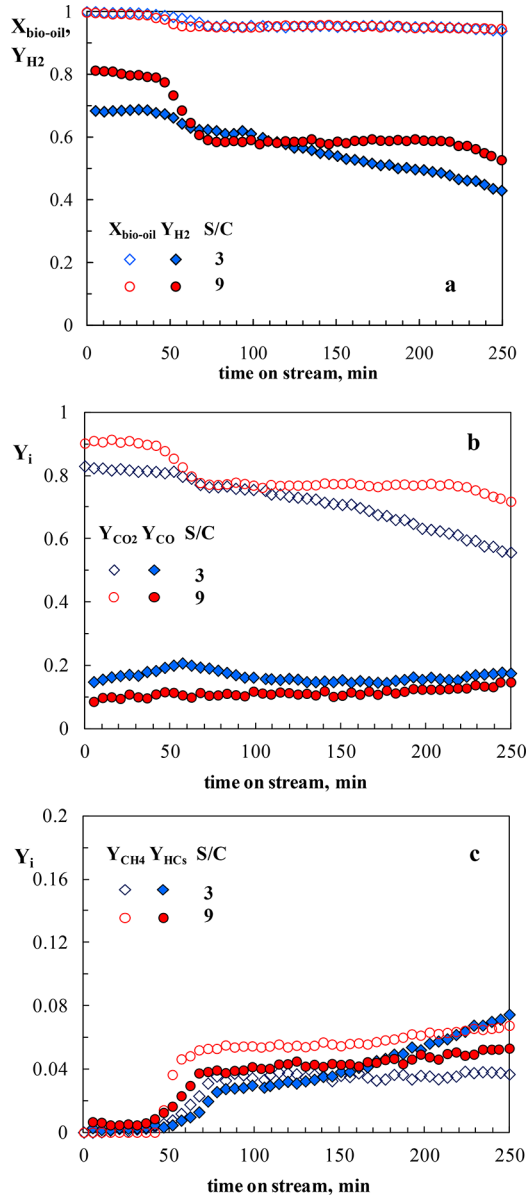

Figure 3. Effect of S/C molar ratio on the evolution with TOS on bio-oil oxygenates conversion and H_2 yield (a) and on the yields of carbon-containing products (b and c). Reaction conditions: 700 °C; O/C, 0.34; space time, 0.15 $g_{catalyst}$ $h/g_{bio\text{-}oil}$.

allowing us to interpret the results obtained in section 3.1 and to identify the causes of deactivation.

3.2.1. Coke Deactivation. The catalysts deactivated under different conditions have been characterized by TPO in order to relate the nature and the content of the coke to the corresponding deactivation results in section 3.1.

Figure 4 shows TPO profiles for different reaction temperatures and space times at an O/C molar ratio of 0.34 and S/C of 6. The results shown in Figure 5 correspond to different S/C molar ratio, temperature, and space time values for an O/C of 0.34. In all the reaction runs the catalyst was used for 4 h TOS. The TPO profiles evidence two combustion peaks: The first peak has a maximum at 300 °C, and a shoulder is observed at slightly higher temperatures under conditions with high deactivation (low values of temperature, space time and S/C ratio). The second peak has its maximum at around 400−410 °C. According to the literature on oxygenates reforming on

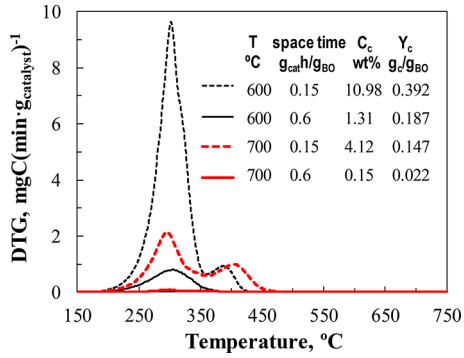

Figure 4. Effect of space time and temperature on the TPO profiles for the catalyst. Reaction conditions: O/C, 0.34; S/C, 6; TOS, 4 h.

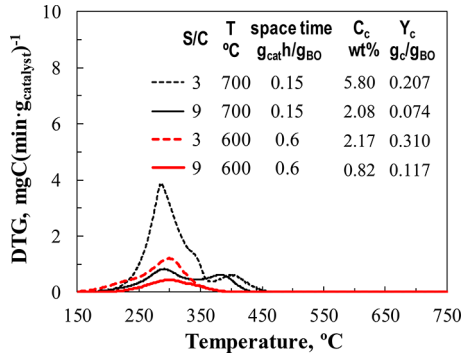

Figure 5. Effect of S/C molar ratio on the TPO profiles for the catalyst deactivated in OSR of bio-oil at two different values of temperature and space time. Reaction conditions: O/C, 0.34; TOS, 4 h.

different catalysts,[40,47−51] it is well-established that the peak at low temperature corresponds to the amorphous coke deposited on metal sites (encapsulating coke), whose combustion is activated by these sites, and which is formed mainly by repolimerization and/or decomposition of unstable oxygenates in the bio-oil. The peak at high temperature corresponds to the coke deposited on the support and is a structured coke containing a significant amount of condensed polyaromatics, whose formation mechanism is related to the decomposition of CH_4 and byproduct hydrocarbons. The presence of a shoulder in the 300−350 °C region suggests the existence of another coke fraction, deposited near the metal−support interphase, whose combustion is favored by the proximity of the metal.[40,49]

Figure 4 shows that the total coke content is lower when the space time is increased. At 700 °C, this decrease is from 4.12 wt % at 0.15 $g_{catalyst}$ $h/g_{bio\text{-}oil}$ to 0.15 wt % at 0.6 $g_{catalyst}$ $h/g_{bio\text{-}oil}$, and for this space time value just an incipient formation of the first peak is observed in the coke combustion curve. The effect of space time on coke deposition is in line with its effect on the attenuation of catalyst deactivation observed in Figure 1. Thus, the increase in space time involves both a significant decrease in coke deposition and a noticeable delay in the catalyst deactivation. Consequently, at 700 °C and for the higher value of space time studied, the deposition of coke is almost insignificant (0.15 wt % after 4 h time on stream), and the second deactivation period is not observed even after 24 h time on stream.[40] These results allow us to conclude that coke deposition is the main cause responsible for the second deactivation period. The effect space time has on the content and nature of coke is explained by the lower concentration of oxygenates in the reaction medium due to the higher

DOI: 10.1021/acs.energyfuels.7b04141
Energy Fuels 2018, 32, 3588−3598

conversion of these oxygenates (Figure 1a). A previous work[48] proves that the compounds in the reaction medium are the precursors for the formation of both coke fractions. Therefore, the oxygenates of the bio-oil have been established as precursors of the encapsulating coke, which is burned at lower temperature. Likewise, the negligible structured coke deposition at high space time is consistent with the lower amount of hydrocarbons present in the reaction medium (Figure 1c), which are considered the main precursors of structured coke formation via condensation reactions.[48] Accordingly, TPO profiles for different space times shown in Figure 5 also demonstrate the attenuating effect of space time on coke deposition.

Figure 4 also shows a remarkable effect of the reforming temperature on the coke nature and content. As observed, an increase in temperature from 600 to 700 °C noticeably attenuates the formation of the first combustion peak (encapsulating coke), which is consistent with the lower deactivation rate observed at 700 °C compared to that at 600 °C (blue dots in Figures 1 and 2, respectively). A decrease in the encapsulating coke deposition when increasing temperature is explained, on the one hand, by the lower concentration of oxygenates in the reaction medium (encapsulating coke precursors) due to the higher conversion along 4 h TOS (Figure 1a) and, on the other hand, by the higher gasification and/or oxidation rate of coke intermediates as they are being formed (reactions activated by Rh active sites). The high deposition of encapsulating coke at 600 °C in Figure 4 is presumably the main cause of the presence of only one deactivation period in Figure 2 at this temperature. Furthermore, Figure 4 shows that an increase in the reforming temperature hardly affects the content of structured coke, but its combustion is displaced toward higher temperature when increasing the reforming temperature from 600 to 700 °C, which is evidence that it is a more condensed coke, with lower H/C ratio, because condensation reactions (aging) of polyaromatic fractions of coke are favored.[48] This result evidences that the structured coke does not block Rh sites and thus has almost no impact on catalyst deactivation. This corroborates the previous conclusion that the encapsulating coke is the main cause responsible for Rh/CeO_2-ZrO_2 catalyst deactivation.[40]

Regarding the effect of S/C ratio on the amount and nature of coke, Figure 5 shows that an increase in S/C ratio selectively affects the formation of encapsulating coke (peaks at lower temperature in the TPO profile), which is explained by the enhancement of oxygenates reforming, which are the precursors of this coke fraction. It is also suggested that an increase in the S/C ratio is effective for boosting the progress of reforming/gasification reactions of coke intermediates deposited on the metallic Rh sites. This hypothesis confirms the fact that the amount of structured coke deposition is not attenuated, because this coke is not in close contact with Rh sites. Moreover, Figure 5 shows that the top of the peak shifts toward lower temperatures as the S/C ratio is increased, which is explained by a high steam content that hinders condensation reactions (aging) of the coke.

3.2.2. Change in the State of Rh Species. The possible changes in Rh species have been analyzed by comparing the H_2-TPR analysis of the deactivated catalysts with that corresponding to the fresh one. It should be noted that using other characterization techniques, such as XRD and X-ray photoelectron spectroscopy (XPS), for analyzing the changes in Rh metal species is difficult. On the one hand, because of the high dispersion and low Rh content (2 wt %), Rh^0 and Rh_2O_3 peaks are not detected by XRD. On the other hand, coke deposition on the deactivated catalysts hinders the detection of Rh^0 and Rh_2O_3 by XPS.

Figure 6 compares the TPR profiles for the fresh (curve a) and deactivated catalysts in runs of 40 and 240 TOS (curves c and d, respectively). These runs were carried out under the following conditions: 700 °C; space time, 0.15 $g_{catalyst}$ $h/g_{bio\text{-}oil}$; S/C ratio, 6; O/C ratio, 0.34. The deactivation results corresponding to these conditions are depicted with blue dots in Figure 1. Three reduction peaks are observed for the fresh catalyst in Figure 6, at 65, 200, and 345 °C. The peaks below 200 °C have been assigned in the literature to the reduction of Rh species, whereas peaks above this temperature are assigned to the reduction of the support.[52−59] Consequently, the peak at 345 °C can be associated with the reduction of surface CeO_2 species in the support, whose reduction is greatly promoted by the presence of Rh, because of a strong $Rh-CeO_2$ interaction and the spillover phenomena.[52,54,55,59] The two peaks observed below 200 °C indicate that Rh species exist in two different states. There is a general agreement in the literature that the peak at the lower reduction temperature corresponds to the reduction of well-dispersed and uniformly distributed rhodium oxides (Rh_2O_3 to Rh^0), which interact very weakly with the support.[52−60] The Rh reduction peak at higher temperature has been attributed by some authors to a bulklike crystalline Rh_2O_3 on the surface (large particles),[52,53,56] whereas a peak at around 200 °C was related to the sublattice rhodium oxides interacting with the support for a Rh/ZrO_2 catalyst.[59,61]

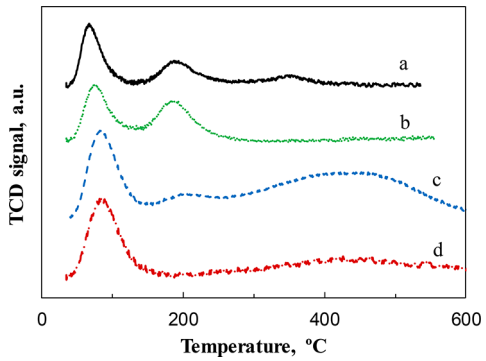

Figure 6. TPR profiles of fresh catalyst (a), after reduction and storing at room conditions (b), and after 40 min TOS (c) and 240 min (d) TOS. Reaction conditions: 700 °C; space time, 0.15 $g_{catalyst}$ $h/g_{bio\text{-}oil}$; O/C, 0.34; S/C, 6.

For the interpretation of the TPR profiles of the spent catalysts, apart from the possible transformations during the reaction itself, possible additional changes must be taken into account in the oxidation state of the spent catalyst when exposed to room conditions prior to the TPR analysis. In order to study the latter phenomenon, TPR of the fresh and reduced catalyst was carried out after exposure to room conditions overnight. Results are shown in curve b in Figure 6, which depicts that the peak associated with the reduction of surface CeO_2 is absent (ceria is not reoxidized at room conditions), whereas both peaks corresponding to the reduction of Rh species appear, which is evidence of their oxidation by exposure to room conditions.

DOI: 10.1021/acs.energyfuels.7b04141
Energy Fuels 2018, 32, 3588−3598

The main difference in the TPR profiles between the catalysts deactivated for 40 and 240 min TOS at low space time (curves c and d, respectively) and the fresh one is that the peak at 200 °C almost disappears for 40 min and is not present for 240 min TOS. This result is probably due to the diffusion of Rh species into the support, which originates a decrease in the content of surface rhodium species.[59] Other possible explanations may be related to the decoration phenomena produced by reduced support particles, which migrate on the top of metal particles, or the encapsulation of metal particles due to support sintering at the high temperatures used for the reforming.[53] Because this change in the structure of Rh species in the catalyst occurs from very low TOS values (40 min, curve c in Figure 6), this is claimed to be the main cause of deactivation for the first deactivation period (first sharp change) at low space time (blue dots in Figure 1). Figure 6 also shows that the reduction peak at lower temperature (oxidation of well-dispersed rhodium oxides to metallic Rh^0) for both spent catalysts is very similar, although it is shifted toward slightly higher temperature (90 °C) compared to the fresh catalyst. This shift of the peak was associated with the reduction of relatively more stable bulklike crystalline rhodium oxide on the sample with bigger particle sizes.[58]

Additionally, it should be noted that the effect of operation conditions on the structural change of Rh species in the deactivated catalyst is much smaller than the effect on coke deposition. Thus, all deactivated samples (after exposure to room conditions) have a similar and unique Rh_2O_3 reduction peak at 90 °C (Figure S1 in the Supporting Information). This result is consistent with the fact that the first deactivation period in Figures 1−3 (which is associated with the deactivation by structural changes in Rh species, as evidenced by the aforementioned results) is much less affected by operating conditions than the second deactivation period (which is associated mainly with coke deactivation).

3.2.3. Sintering of Rh. It is remarkable that an almost negligible encapsulating coke combustion peak is observed in the TPO profiles of the catalyst deactivated at 750 °C (Figure S2). Consequently, the slow and continuous deactivation in Figure 2 for the catalyst at 750 °C after the first deactivation period (caused by structural changes in Rh species) should be attributed to deactivation causes other than coke deposition, such as Rh metal particle sintering occurring at this high temperature under oxidizing conditions. The sintering of Rh under highly oxidizing conditions was reported by Cavallaro et al.[62] for a 5 wt %Rh/Al_2O_3 catalyst used in autothermal reforming of ethanol at 650 °C. However, the CeO_2 support is expected to attenuate sintering, as proven by Osorio-Vargas et al.[63] by addition of CeO_2 to a Rh/Al_2O_3−LaO_3 catalyst, and Hou et al.[64] with a Rh/CeO_2 catalyst. A previous work[40] proved that sintering of Rh/CeO_2−ZrO_2 catalyst used in this study is not significant in long runs below 700 °C.

In order to confirm this hypothesis that Rh sintering is the main deactivation cause at 750 °C, TEM images are shown in Figure 7 for the fresh catalyst and the one deactivated for 4 h TOS at two temperatures (600 and 750 °C) (and for the remaining operating conditions shown in Figure 2). Furthermore, the particle size distribution (PSD) results for each catalyst sample, obtained by counting more than 200 particles, are also shown in this figure, together with the corresponding average size, evaluated as the arithmetic mean of all the particles counted. The average size is 1.36 nm for the fresh catalyst and 1.42 and 2.58 nm for the catalyst spent at 600 and 750 °C,

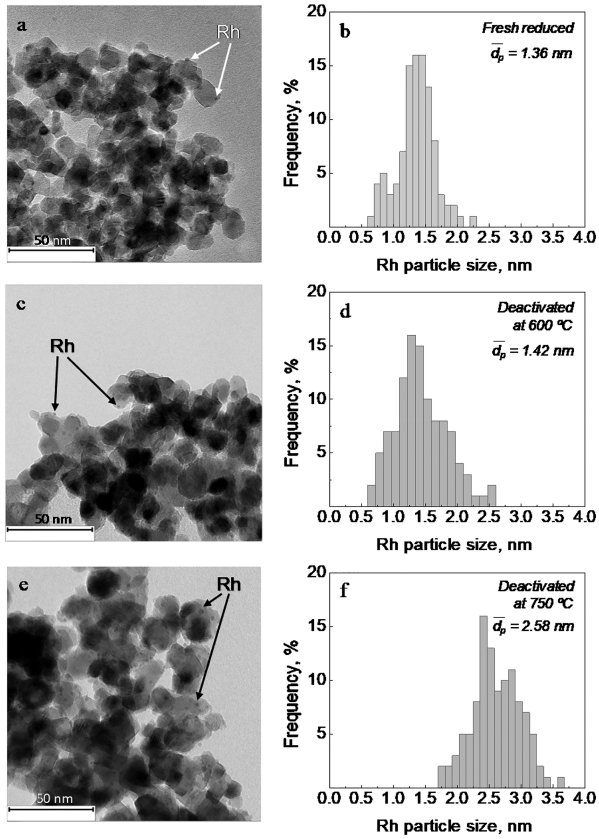

Figure 7. TEM images and particle size distribution (PSD) of fresh catalyst (a and b) and of deactivated catalyst at 600 °C (c and d) and 750 °C (e and f). Reaction conditions: space time, 0.15 $g_{catalyst}$ h/$g_{bio\text{-}oil}$; O/C, 0,34; S/C, 6.

respectively. These results are evidence of a remarkable sintering of Rh particles at 750 °C (with an increase in the average metal particle size of 90%), which is the main cause of the slight deactivation observed in Figure 2 at this temperature after the first sharp change. This deactivation cannot be attributed to coke deposition because this is negligible at 750 °C (Figure S2). At 700 °C (Figure S3) sintering is incipient but progresses with time, and the average particle size is 2.26 nm after 24 h TOS.

Accordingly, catalyst deactivation at 600−750 °C is governed by coke deposition at low temperature and Rh sintering at high temperature. By comparing the deactivation observed at 600 °C in Figure 2 (attributable to coke deposition) with that obtained at 750 °C in the second deactivation period (attributed to sintering), it is evident that the deactivation caused by encapsulating coke deposition is more severe than the deactivation caused by sintering.

3.2.4. Change in the Porous Structure of the Support. In order to evaluate the contribution to the deactivation of the possible deterioration of the porous structure of the CeO_2−ZrO_2 support, the surface properties of the deactivated catalyst have been studied by means of N_2 adsorption−desorption under some chosen conditions as an example. The results in Table 1 show that the surface properties of the catalyst undergo remarkable deterioration in the reduction step, and especially during the reaction step. This deterioration depends on the reaction conditions. The possible causes for this deterioration of the surface can be the deposition of coke and the aging of the support. The similarity of Brunauer−Emmett−Teller (BET)

DOI: 10.1021/acs.energyfuels.7b04141
Energy Fuels 2018, 32, 3588−3598

Table 1. BET Surface Area, Pore Volume, and Mean Pore Diameter of the $Rh/CeO_2–ZrO_2$ Catalyst Deactivated at Different Temperatures and S/C Ratios and of the Reduced Catalyst[a]

T (°C)	S/C	S_{BET} ($m^2\ g^{-1}$)	V_{pore} ($cm^3\ g^{-1}$)	D_{pore} (nm)
600	6	47.1	0.187	15.9
700	6	37.9	0.163	17.2
750	6	41.2	0.184	17.9
700	3	38.5	0.167	17.4
700	9	43.3	0.180	16.6
reduced (700 °C, 2 h)		76.0	0.261	19.2

[a]Reaction conditions: O/C = 0.34; space time = 0.15 $g_{catalyst}\ h/g_{bio\text{-}oil}$.

surface and pore volume values for the catalyst deactivated at 750 °C (and therefore, without coke deposition) and those deactivated at 700 °C (with variable contents of coke according to the S/C ratio) evidences that the deposition of coke has a negligible impact on the porous structure and that these changes must be attributed mainly to the aging of the $CeO_2–ZrO_2$ support. In addition, the comparison of the results for the catalyst deactivated at different temperatures shows that the increase in temperature significantly affects this aging of the support, especially between 600 and 700 °C. The importance of the aging of the support at high temperature (with notable loss of specific surface area) is well-established in the literature for catalysts based on CeO_2 and $CeO_2–ZrO_2$.[65,66]

It should be noted that presumably the aging of the support will lead to the partial occlusion of Rh metal sites, contributing to the structural changes in Rh which are shown in section 3.2.2 and the progress of deactivation in the first period of fast deactivation shown in Figures 1–3.

4. DISCUSSION

From the results shown in Figures 1–3, it is concluded that the evolution of reaction indices with TOS in the OSR of raw bio-oil on a $Rh/CeO_2–ZrO_2$ catalyst follows the general trend shown in Figure 8. CO_2 yield evolution is not shown because it goes almost parallel to H_2 yield evolution. Likewise, CO yield evolution is not shown either because it does not show a similar trend for all the operating conditions studied, although in general the variation of CO yield with TOS is negligible and slow. This could be partially attributed to the presence of CeO_2 in the support, whose interaction with Rh species enhances the WGS reaction.

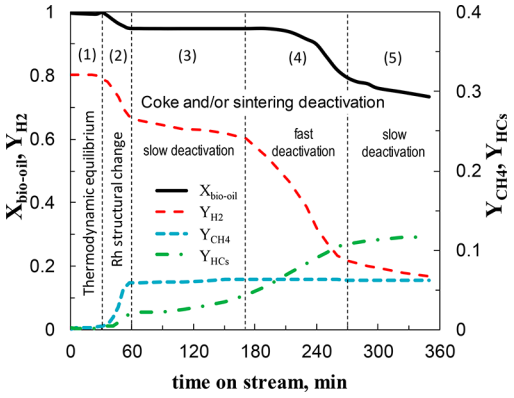

Figure 8. Deactivation steps and typical evolution with TOS of bio-oil oxygenates conversion and yields of products in OSR of the bio-oil with $Rh/CeO_2–ZrO_2$ catalyst.

Five successive stages and catalyst states are identified in Figure 8 with two well-differentiated fast deactivation periods (sharp changes). The first period (1) takes place under conditions in which thermodynamic equilibrium is achieved and the reaction indices are maintained at equilibrium values. During this period, excess catalyst masks deactivation. Next, a short period of fast deactivation (2) occurs, and subsequently a new pseudostable state is reached (3), in which the catalyst still keeps high activity. Period 4 corresponds to a fast catalyst deactivation, thus rapidly decreasing H_2 and CO_2 and increasing HCs yields. The variation rate of the reaction indices decreases when increasing the TOS. During period 5, the catalyst undergoes a high deactivation level; therefore, the variation in the reaction indices takes place slowly as they reach the values corresponding to thermal routes. Although the catalyst is almost completely deactivated for the reforming reactions during this period (5), it still keeps a remarkable residual activity for cracking of oxygenates and the WGS reaction. This residual activity for the WGS reaction should be attributed to the interaction of $CeO_2–ZrO_2$ support with the Rh active sites. The important role of metal–surface interface sites for the WGS reaction has been reported in the literature.[46,67]

It should be noted that Figure 8 considers the global conversion of bio-oil oxygenates; however, in fact, this conversion is a consequence of the individual conversion of each of the oxygenates, whose reforming rate is different and is selectively affected by deactivation. Thus, Figure S4 shows the effect of the deactivation on the molar fraction distribution of oxygenate families at the reactor outlet for a set of conditions chosen as an example. The results in Figure S4 show that phenolic oxygenates are the most abundant oxygenates under conditions of low catalyst deactivation (periods 1, 2, and 3 of Figure 8), which occur before the second period of rapid deactivation. The fast increase with the time on stream of the concentration of phenols at the reactor outlet, under conditions of incipient deactivation, evidence the selective deactivation of the reforming for the most refractory compounds.

On the other hand, the conversion of water is low for most of the studied conditions (with excess of water), with values that vary at zero time on stream between 0.15 and 0.07 for S/C ratio between 3 and 9, respectively. The evolution with the time on stream of this conversion has a trend similar to that of the conversion of oxygenates in bio-oil, decreasing because of the catalyst deactivation, until reaching negative values under conditions of very high deactivation (corresponding to period 5 in Figure 8). This is due to the fact that under these conditions the water formation in the oxidation reactions is favored over its consumption in the reforming and WGS reactions.

According to the analysis of coke and Rh active sites, both sharp changes in Figure 8 might be related to three different catalyst deactivation causes: structural changes of Rh species and of the support, coke deposition, and Rh sintering. These causes evolve differently with TOS, depending on the reaction conditions (temperature, space time, S/C ratio, and O/C ratio), and their relative importance depends therefore on the reaction conditions. The first sharp change stems from a fast change in the structure of Rh species and in the support, which leads to selective catalyst deactivation for the reforming of the less reactive compounds (CH_4 and phenols) keeping high activity for the rest of the reactions (reforming of non-phenolic

DOI: 10.1021/acs.energyfuels.7b04141
Energy Fuels 2018, 32, 3588–3598

Table 2. Qualitative Effect of the Increase in the Different Operating Conditions on the Initial H_2 Yield and on the Different Causes of $Rh/CeO_2–ZrO_2$ Catalyst Deactivation

	temperature (600–750 °C)	space time (0.15–0.60 $g_{catalyst}$ h/$g_{bio\text{-}oil}$)	S/C ratio (3–9)	O/C ratio[40] (0–0.67)
H_2 yield	↓	↑	↑↑	↓↓↓
Rh structural change	↑	=	↑	↑
Rh sintering	↑↑	*a*	*a*	*a*
coke deposition				
encapsulating	↓↓↓	↓↓↓↓	↓↓	↓↓↓
structured	=	↓↓↓↓	=	↓↓

[a]Not studied.

oxygenates and hydrocarbons and WGS reaction).[40] This deactivation cause is barely affected by the reaction conditions. Deactivation during periods 3–5 might be related to two simultaneous deactivation causes, coke deposition, and/or Rh sintering, the former being the main cause responsible for the second sharp change (period 4). The pseudostable period prior to this sharp change is attributed to the need of an initiation step for the formation of encapsulating coke via polymerization of the phenolic compounds in the bio-oil.[48] Under high deactivating conditions due to rapid encapsulating coke deposition (as happens at 600 °C and low space time) this cause masks the changes in the structure of Rh species, and consequently a single and very pronounced sharp change is observed. At high temperature (750 °C), the encapsulating coke formation is negligible and the progressive Rh sintering becomes significant, which is the main deactivation cause after the first sharp change under these conditions. Rh sintering has a progressive effect on the evolution of the reaction indices with TOS. However, the latter effect is less significant than that due to the encapsulating coke deposition at low temperature, giving place to a slow decrease in conversion and H_2 yield with TOS, which is visible at low space time (red dots in Figure 2).

Moreover, in order to understand the resulting product distribution, it should be noted that incomplete and complete combustion of compounds in the reaction medium (H_2, CH_4, hydrocarbons, oxygenates, and CO) contribute to the formation of CO and CO_2, although the rate of these reactions is presumably hardly affected by catalyst deactivation compared to reforming and WGS reactions.

According to the results in section 3, the reaction conditions should be established in order to minimize all different deactivation causes. Table 2 summarizes the effect of each reaction condition (temperature, space time, and S/C and O/C ratios) on the H_2 yield and different deactivation causes. Deactivation due to changes in the structure of Rh species is hardly affected by reaction conditions, although according to Figures 2 and 3 it seems to be slightly attenuated when decreasing temperature and S/C and O/C ratios.[40] Coke deposition is remarkably attenuated when increasing temperature and S/C and O/C ratios (conditions favoring the reforming of oxygenates and the combustion and gasification of the coke precursors absorbed on metallic sites).[40] Although coke deposition is almost completely avoided at 750 °C, deactivation at this temperature due to Rh sintering becomes significant, almost doubling the Rh particle size after 4 h TOS.

Consequently, in order to obtain a good compromise between the maximum H_2 yield and catalyst stability, 700 °C is the optimum temperature. The remaining conditions will be determined according to economic viability studies and will depend on the working scale. However, the conditions required for high catalytic stability are high space time, O/C ratio in the 0.34–0.67 range (the latter corresponding to the autothermal regime), and moderate S/C ratio (around 6, in order to moderate water consumption for water vaporization).

5. CONCLUSIONS

Rh supported on $CeO_2–ZrO_2$ has a good kinetic behavior for the oxidative reforming of bio-oil. For an O/C ratio of 0.34, the catalyst shows full conversion of bio-oil oxygenates at zero TOS in the whole range of conditions studied (600–750 °C; space time, 0.15–0.6 $g_{catalyst}$ h/$g_{bio\text{-}oil}$; S/C ratio, 3–9), and high initial H_2 yield (between 70 and 80%), low initial CO yield (below 16%) and insignificant CH_4 and hydrocarbons yields.

Catalyst stability is affected by three different deactivation causes: (i) change in the structure of Rh species and their interaction with the support (which suffers aging during the reaction), (ii) encapsulating coke deposition, and (iii) Rh sintering. They all appear throughout the reaction, and both their relative importance and evolution depend on the reaction conditions. Consequently, the evolution of bio-oil oxygenates conversion and yields of products with TOS may show two consecutive sharp changes. The first change is a consequence of changes in the structure of Rh species and in the support (hardly affected by the operating conditions in the range studied), and it affects to a greater extent the reforming of refractory oxygenates (phenols) and CH_4. The second change is mainly due to the formation of encapsulating coke, with the effect of Rh sintering being steadily increasing. Coke deposition is considerably attenuated by increasing S/C ratio and, particularly, when temperature is increased, being negligible at 750 °C, even though Rh sintering becomes significant at 750 °C.

Consequently, the optimum conditions for the OSR of bio-oil over $Rh/CeO_2–ZrO_2$ catalyst, to strike a balance between high H_2 yield and high catalyst stability, correspond to 700 °C, with high space time (>0.6 $g_{catalyst}$ h/$g_{bio\text{-}oil}$), and moderate S/C ratio (around 6, in order to avoid excessive energy requirement for water vaporization).

■ ASSOCIATED CONTENT

Supporting Information

The Supporting Information is available free of charge on the ACS Publications website at DOI: 10.1021/acs.energyfuels.7b04141.

TPR and TPO profiles for the catalyst under different conditions, TEM image and PSD of the catalyst, and evolution with TOS of the molar fraction of oxygenates (PDF)

DOI: 10.1021/acs.energyfuels.7b04141
Energy Fuels 2018, 32, 3588–3598

AUTHOR INFORMATION

Corresponding Author

*E-mail: aingeru.remiro@ehu.es.

ORCID

Aingeru Remiro: 0000-0002-6746-3021

Notes

The authors declare no competing financial interest.

ACKNOWLEDGMENTS

This work was carried out with the financial support of the Department of Education Universities and Investigation of the Basque Government (IT748-13), the Ministry of Economy and Competitiveness of the Spanish Government jointly with the European Regional Development Funds (AEI/FEDER, UE) (Proyects CTQ2012-35263 and CTQ2015-68883-R and Ph.D. Grant BES-2013-063639 for A.A.), and the European Union's Horizon 2020 research and innovation programme under the Marie Skłodowska-Curie Grant Agreement No. 704473.

NOMENCLATURE

C_C = coke content, wt % referred to mass of catalyst
F_{in}, F_{out} = molar flow rate of bio-oil oxygenates at the reactor inlet and outlet, respectively, in C equivalent units, mol h^{-1}
F_i = molar flow rate of i carbon-containing product at the reactor outlet, in C equivalent units, mol h^{-1}
F_{H_2} = molar flow rate of H_2 at the reactor outlet, mol h^{-1}
$F^0_{H_2}$ = stoichiometric molar flow rate of H_2 at the reactor outlet, for SR, mol h^{-1}
O/C = oxygen-to-carbon ratio
PSD = particle size distribution
S/C = steam-to-carbon ratio
TOS = time on stream
$X_{bio\text{-}oil}$ = conversion of bio-oil oxygenates
Y_C = coke yield, $g_{coke}\ g_{bio\text{-}oil}^{-1}$
Y_{H_2} = hydrogen yield
Y_i = yield of i carbon-containing product (CO, CO_2, CH_4, C_2–C_4)

REFERENCES

(1) Ellabban, O.; Abu-Rub, H.; Blaabjerg, F. *Renewable Sustainable Energy Rev.* **2014**, *39*, 748–764.
(2) Levalley, T. L.; Richard, A. R.; Fan, M. *Int. J. Hydrogen Energy* **2014**, *39*, 16983–17000.
(3) Dincer, I.; Acar, C. *Int. J. Hydrogen Energy* **2015**, *40*, 11094–11111.
(4) Nabgan, W.; Tuan Abdullah, T. A.; Mat, R.; Nabgan, B.; Gambo, Y.; Ibrahim, M.; Ahmad, A.; Jalil, A. A.; Triwahyono, S.; Saeh, I. *Renewable Sustainable Energy Rev.* **2017**, *79*, 347–357.
(5) Bridgwater, A. V. *Biomass Bioenergy* **2012**, *38*, 68–94.
(6) Xiu, S.; Shahbazi, A. *Renewable Sustainable Energy Rev.* **2012**, *16*, 4406–4414.
(7) Meier, D.; van de Beld, B.; Bridgwater, A. V.; Elliott, D. C.; Oasmaa, A.; Preto, F. *Renewable Sustainable Energy Rev.* **2013**, *20*, 619–641.
(8) Carpenter, D.; Westover, T. L.; Czernik, S.; Jablonski, W. *Green Chem.* **2014**, *16*, 384–406.
(9) Amutio, M.; Lopez, G.; Aguado, R.; Artetxe, M.; Bilbao, J.; Olazar, M. *Energy Fuels* **2011**, *25*, 3950–3960.
(10) Amutio, A.; Lopez, G.; Aguado, R.; Bilbao, J.; Olazar, M. *Energy Fuels* **2012**, *26*, 1353–1362.
(11) Kechagiopoulos, P. N.; Voutetakis, S. S.; Lemonidou, A. A.; Vasalos, I. A. *Energy Fuels* **2006**, *20*, 2155–2163.
(12) Czernik, S.; Evans, R.; French, R. *Catal. Today* **2007**, *129*, 265–268.
(13) Sarkar, S.; Kumar, A. *Bioresour. Technol.* **2010**, *101*, 7350–7361.
(14) Zhang, Y.; Brown, T. R.; Hu, G.; Brown, R. C. *Biomass Bioenergy* **2013**, *51*, 99–108.
(15) Czernik, S.; French, R. *Int. J. Hydrogen Energy* **2014**, *39*, 744–750.
(16) Remiro, A.; Valle, B.; Aguayo, A. T.; Bilbao, J.; Gayubo, A. G. *Energy Fuels* **2013**, *27*, 7549–7559.
(17) Valle, B.; Remiro, A.; Aramburu, B.; Bilbao, J.; Gayubo, A. G. *J. Cleaner Prod.* **2015**, *88*, 345–348.
(18) Rioche, C.; Kulkarni, S.; Meunier, F. C.; Breen, J. P.; Burch, R. *Appl. Catal., B* **2005**, *61*, 130–139.
(19) Medrano, J. A.; Oliva, M.; Ruiz, J.; García, L.; Arauzo, J. *Int. J. Hydrogen Energy* **2008**, *33*, 4387–96.
(20) Trane, R.; Dahl, S.; Skjoth-Rasmussen, M. S.; Jensen, A. D. *Int. J. Hydrogen Energy* **2012**, *37*, 6447–6472.
(21) Vagia, E. C.; Lemonidou, A. A. *Int. J. Hydrogen Energy* **2008**, *33*, 2489–500.
(22) Youn, M. H.; Seo, J. G.; Cho, K. M.; Park, S.; Park, D. R.; Jung, J. C.; Song, I. K. *Int. J. Hydrogen Energy* **2008**, *33*, 5052–5059.
(23) Chakrabarti, R.; Tupy, S. A.; Schmidt, L. D. *Energy Fuels* **2011**, *25*, 4763–4769.
(24) Graschinsky, C.; Lupiano-Contreras, J.; Amadeo, N.; Laborde, M. *Ind. Eng. Chem. Res.* **2014**, *53*, 15348–15356.
(25) Mondal, T.; Pant, K. K.; Dalai, A. K. *Int. J. Hydrogen Energy* **2015**, *40*, 2529–2544.
(26) Espitia-Sibaja, M.; Muñoz, M.; Moreno, S.; Molina, R. *Fuel* **2017**, *194*, 7–16.
(27) Mawdsley, J. R.; Krause, T. R. *Appl. Catal., A* **2008**, *334*, 311–320.
(28) Amjad, U. E. S.; Vita, A.; Galletti, C.; Pino, L.; Specchia, S. *Ind. Eng. Chem. Res.* **2013**, *52*, 15428–15436.
(29) Malaibari, Z. O.; Amin, A.; Croiset, E.; Epling, W. *Int. J. Hydrogen Energy* **2014**, *39*, 10061–10073.
(30) Silva, P. P.; Ferreira, R. A. R.; Noronha, F. B.; Hori, C. E. *Catal. Today* **2017**, *289*, 211–221.
(31) Hu, X.; Lu, G. *Appl. Catal., B* **2010**, *99*, 289–297.
(32) Kamonsuangkasem, K.; Therdthianwong, S.; Therdthianwong, A. *Fuel Process. Technol.* **2013**, *106*, 695–703.
(33) Paasikallio, V.; Azhari, A.; Kihlman, J.; Simell, P.; Lehtonen, J. *Int. J. Hydrogen Energy* **2015**, *40*, 12088–12096.
(34) Rennard, D.; French, R.; Czernik, S.; Josephson, T.; Schmidt, L. *Int. J. Hydrogen Energy* **2010**, *35*, 4048–4059.
(35) Salehi, E.; Seyedeyn-Azad, F.; Harding, T.; Abedi, J. *Fuel Process. Technol.* **2011**, *92*, 2203–2210.
(36) Seyedeyn-Azad, F.; Abedi, J.; Harding, T. *Chem. Eng. J.* **2012**, *180*, 145–150.
(37) Li, D.; Li, X.; Gong, J. *Chem. Rev.* **2016**, *116*, 11529–11653.
(38) Fierro, V.; Akdim, O.; Provendier, H.; Mirodatos, C. *J. Power Sources* **2005**, *145*, 659–666.
(39) Chiodo, V.; Freni, S.; Galvagno, A.; Mondello, N.; Frusteri, F. *Appl. Catal., A* **2010**, *381*, 1–7.
(40) Remiro, A.; Arandia, A.; Bilbao, J.; Gayubo, A. G. *Energy Fuels* **2017**, *31*, 7147–7156.
(41) Arandia, A.; Remiro, A.; Bilbao, J.; Gayubo, A. G. *Int. J. Hydrogen Energy* **2017**, *42*, 29175–29185.
(42) Fernández-Akarregi, A. R.; Makibar, J.; López, G.; Amutio, M.; Olazar, M. *Fuel Process. Technol.* **2013**, *112*, 48–56.
(43) Ochoa, A.; Aramburu, B.; Ibañez, M.; Valle, B.; Bilbao, J.; Gayubo, A. G.; Castaño, P. *ChemSusChem* **2014**, *7*, 2597–2608.
(44) Valle, B.; Aramburu, B.; Arandia, A.; Remiro, A.; Bilbao, J.; Gayubo, A. G. *Chem. Eng. Trans.* **2017**, *57*, 205–210.
(45) Arandia, A.; Remiro, A.; Valle, B.; Bilbao, J.; Gayubo, A. G. *Chem. Eng. Trans.* **2017**, *57*, 217–222.
(46) Roh, H.-S.; Potdar, H. S.; Jeong, D.-W.; Kim, K.-S.; Shim, J.-O.; Jang, W.-J.; Koo, K. Y.; Yoon, W. L. *Catal. Today* **2012**, *185*, 113–118.
(47) Remiro, A.; Valle, B.; Aguayo, A. T.; Bilbao, J.; Gayubo, A. G. *Fuel Process. Technol.* **2013**, *115*, 222–232.
(48) Ochoa, A.; Aramburu, B.; Valle, B.; Resasco, D. E.; Bilbao, J.; Gayubo, A. G.; Castaño, P. *Green Chem.* **2017**, *19*, 4315–4333.

DOI: 10.1021/acs.energyfuels.7b04141
Energy Fuels 2018, 32, 3588–3598

(49) Martin, N.; Viniegra, M.; Lima, E.; Espinosa, G. *Ind. Eng. Chem. Res.* **2004**, *43*, 1206−1210.
(50) Vicente, J.; Montero, C.; Ereña, J.; Azkoiti, M. J.; Bilbao, J.; Gayubo, A. G. *Int. J. Hydrogen Energy* **2014**, *39*, 12586−12596.
(51) Montero, C.; Ochoa, A.; Castaño, P.; Bilbao, J.; Gayubo, A. G. *J. Catal.* **2015**, *331*, 181−192.
(52) Fornasiero, P.; Di Monte, R.; Ranga Rao, G.; Kaspar, J.; Meriani, S.; Trovarelli, A.; Graziani, M. *J. Catal.* **1995**, *151*, 168−177.
(53) Diagne, C.; Idriss, H.; Kiennemann, A. *Catal. Commun.* **2002**, *3*, 565−571.
(54) Rocchini, E.; Vicario, M.; Llorca, J.; de Leitenburg, C.; Dolcetti, G.; Trovarelli, A. *J. Catal.* **2002**, *211*, 407−421.
(55) Cai, W.; Wang, F.; Van Veen, A. C.; Provendier, H.; Mirodatos, C.; Shen, W. *Catal. Today* **2008**, *138*, 152−156.
(56) Peela, N. R.; Kunzru, D. *Int. J. Hydrogen Energy* **2011**, *36*, 3384−3396.
(57) Han, X.; Yu, Y.; He, H.; Shan, W. *Int. J. Hydrogen Energy* **2013**, *38*, 10293−10304.
(58) Sharma, P. K.; Saxena, N.; Roy, P. K.; Bhatt, A. *Int. J. Hydrogen Energy* **2016**, *41*, 6123−6133.
(59) Cao, Y.; Ran, R.; Wu, X.; Wan, J.; Weng, D. *Catal. Today* **2017**, *281*, 490−499.
(60) Eriksson, S.; Rojas, S.; Boutonnet, M.; Fierro, J. L. G. *Appl. Catal., A* **2007**, *326*, 8−16.
(61) Zhang, Y.; Kershaw, R.; Dwight, K.; Wold, A. *J. Solid State Chem.* **1988**, *72*, 131−136.
(62) Cavallaro, S.; Chiodo, V.; Vita, A.; Freni, S. *J. Power Sources* **2003**, *123*, 10−16.
(63) Osorio-Vargas, P.; Campos, C. H.; Navarro, R. M.; Fierro, J. L. G.; Reyes, P. *Appl. Catal., A* **2015**, *505*, 159−172.
(64) Hou, T.; Yu, B.; Zhang, S.; Xu, T.; Wang, D.; Cai, W. *Catal. Commun.* **2015**, *58*, 137−140.
(65) Pantu, P.; Gavalas, G. R. *Appl. Catal., A* **2002**, *223*, 253−260.
(66) Mortola, V. B.; Ruiz, J. A. A.; Mattos, L. V.; Noronha, F. B.; Hori, C. E. *Catal. Today* **2008**, *133*−*135*, 906−912.
(67) Aranifard, S.; Ammal, S. C.; Heyden, A. *J. Catal.* **2014**, *309*, 314−324.

DOI: 10.1021/acs.energyfuels.7b04141
Energy Fuels 2018, 32, 3588−3598